Horizontal transport affecting trace gas seasonality in the Tropical Tropopause Layer (TTL)

F. Ploeger,[1] P. Konopka,[1] R. Müller,[1] S. Fueglistaler,[2] T. Schmidt,[3] J. C. Manners,[4] J.-U. Grooß,[1] G. Günther,[1] P. M. Forster,[5] and M. Riese[1]

Received 3 December 2011; revised 21 February 2012; accepted 30 March 2012; published 9 May 2012.

[1] We analyze horizontal transport from midlatitudes into the tropics (in-mixing) and its impact on seasonal variations of ozone, carbon monoxide and water vapor in the Tropical Tropopause Layer (TTL). For this purpose, we use three-dimensional backward trajectories, driven by ECMWF ERA-Interim winds, and a conceptual one-dimensional model of the chemical composition of the TTL. We find that the fraction of in-mixed midlatitude air shows an annual cycle with maximum during NH summer, resulting from the superposition of two inversely phased annual cycles for in-mixing from the NH and SH, respectively. In-mixing is driven by the monsoonal upper-level anticyclonic circulations. This circulation pattern is dominated by the Southeast Asian summer monsoon and, correspondingly, in-mixing shows an annual cycle. The impact of in-mixing on TTL mixing ratios depends on the in-mixed fraction of midlatitude air and on the meridional gradient of the particular species. For CO the meridional gradient and consequently the effect of in-mixing is weak. For water vapor, in-mixing effects are negligible. For ozone, the meridional gradient is large and the contribution of in-mixing to the ozone maximum during NH summer is about 50%. This in-mixing contribution is not sensitive to the tropical ascent velocity, which is about 40% too fast in ERA-Interim. As photochemically produced ozone in the TTL shows no distinct summer maximum, the ozone annual anomaly in the upper TTL turns out to be mainly forced by in-mixing of ozone-rich extratropical air during NH summer.

Citation: Ploeger, F., P. Konopka, R. Müller, S. Fueglistaler, T. Schmidt, J. C. Manners, J.-U. Grooß, G. Günther, P. M. Forster, and M. Riese (2012), Horizontal transport affecting trace gas seasonality in the Tropical Tropopause Layer (TTL), *J. Geophys. Res.*, *117*, D09303, doi:10.1029/2011JD017267.

1. Introduction

[2] The mixing ratios of several trace gas species show distinct seasonal variations in the Tropical Tropopause Layer TTL [see *Fueglistaler et al.*, 2009a]. The trace gas composition of the TTL, in turn, crucially affects the global radiation budget [*Forster and Shine*, 1999; *Solomon et al.*, 2010]. Through their influence on temperatures, trace gas mixing ratios in the TTL have an impact on stratospheric water vapor and chemistry, with implications for global radiation. Consequently, for understanding the changing climate system, it is important to understand the processes controlling the TTL tracer composition. Of particular interest here are those processes involved in the forcing of the seasonality of different species.

[3] Annual cycles are evident in the concentrations of water vapor [*Mote et al.*, 1995], ozone [*Thompson et al.*, 2003; *Folkins et al.*, 2006; *Randel et al.*, 2007] and carbon monoxide [*Schoeberl et al.*, 2006; *Folkins et al.*, 2006; *Randel et al.*, 2010], with the maximum mixing ratios occurring during Northern hemisphere (NH) summer for water vapor and ozone, and during NH winter for carbon monoxide (here and throughout the paper, seasons are defined with respect to the NH). An irregular cycle is found in the concentrations of HCN [*Pumphrey et al.*, 2008; *Randel et al.*, 2010; *Pommrich et al.*, 2010]. The different seasonal variations in the TTL potentially propagate upwards into the stratosphere with the upwelling branch of the stratospheric Brewer-Dobson circulation, creating so-called 'tape recorder' signals [*Mote et al.*, 1996].

[4] Transport between the extratropics and the tropics is suppressed due to the subtropical jets, acting as strong transport barriers. However, observations show that the barrier is to some degree permeable [e.g., *Tuck et al.*, 1997; *Avallone and Prather*, 1997; *Marcy et al.*, 2007]. Weak horizontal (isentropic) transport, both advective and diffusive, occurs in both directions, out of the tropics and from the extratropics into the tropics (termed in-mixing, in the

[1]IEK-7, Institute for Energy and Climate Research, Forschungszentrum Jülich, Jülich, Germany.
[2]Department of Geosciences, Princeton University, Princeton, New Jersey, USA.
[3]GFZ, Potsdam, Germany.
[4]Met Office, Exeter, UK.
[5]Department of Meteorology, University of Reading, Reading, UK.

Corresponding author: F. Ploeger, IEK-7, Institute for Energy and Climate Research, Forschungszentrum Jülich, D-52428 Jülich, Germany. (f.ploeger@fz-juelich.de)

0148-0227/12/2011JD017267

following), with the fraction of midlatitude air in the upper TTL (at about 400 K potential temperature) of around 6% during March/April and October/November [*Volk et al.*, 1996].

[5] *Dunkerton* [1995] and *Chen* [1995] already proposed that exchange between the extratropics and tropics is mainly caused by the monsoon systems, in particular the Asian monsoon during NH summer, comprising large anticyclones in the upper troposphere and lower stratosphere UTLS [cf. also *Randel and Park*, 2006]. *Haynes and Shuckburgh* [2000] showed that, indeed, the transport barrier between the extratropics and tropics weakens during NH summer. In a recent study, *Ray et al.* [2010] emphasized the role of horizontal in-mixing into the tropics for understanding the trends of stratospheric mean age of air and ozone.

[6] However, the forcing mechanisms controlling the trace gas seasonality in the TTL are usually analyzed from a perspective assuming the tropics being isolated against exchange with the extratropics [cf., e.g., *Schoeberl et al.*, 2008]. For water vapor, this one-dimensional tropical perspective is expected to work rather well, as the variations in mixing ratios are mainly related to the annual variation in tropical tropopause temperatures [*Holton and Gettelman*, 2001; *Fueglistaler and Haynes*, 2005; *Schiller et al.*, 2009]. Exchange with the extratropics turns out to be essential for dilution of water vapor tape recorder extrema in the lower stratosphere [*Mote et al.*, 1998], but seems of second order importance for causing the seasonality in the TTL.

[7] The processes which force the seasonality of ozone and carbon monoxide in the tropics are currently debated. For carbon monoxide, *Schoeberl et al.* [2006] related the annual cycle in the TTL to the seasonality of tropospheric sources. On the other hand, *Randel et al.* [2007] emphasized the major role of the annual cycle of tropical Brewer-Dobson circulation upwelling acting on the CO background gradient, with slowest upwelling during NH summer causing less upward transport of CO and lower mixing ratios in the TTL, compared to NH winter.

[8] Also the annual cycle of ozone in the upper TTL, with its maximum during NH summer, was recently explained from different points of view. Using a tropical perspective, *Folkins et al.* [2006] discussed the coupling between vertical circulation and convective outflow, and *Randel et al.* [2007] related the summer maximum in tropical ozone mixing ratios to the seasonality of upwelling acting on the ozone background gradient. In these analyses a complete isolation of the tropics from the extratropics was assumed. *Konopka et al.* [2009, 2010], on the other hand, proposed that there is a seasonality in horizontal transport of ozone-rich extratropical air into the tropics that contributes substantially to the seasonality observed in the TTL.

[9] In this work, we aim to systematically analyze the link between horizontal in-mixing into the tropics and the seasonality of trace gas mixing ratios in the TTL. We disentangle the effects of the seasonality of tropical upward transport, with slowest ascent causing longest transit times into the TTL during NH summer, and of horizontal in-mixing on the seasonality of the TTL composition. Therefore, we use three-dimensional (3D) backward trajectories and a conceptual one-dimensional (1D) tropical model of chemical tracers. The main goals are (i) to investigate the seasonality of in-mixing into the TTL and its forcing mechanism, and (ii) to analyze the impact of in-mixing on the seasonality of water vapor, ozone and carbon monoxide in the TTL. We further discuss how much of the tropical ozone mixing ratio and its annual amplitude can be attributed to in-mixing.

[10] Our analysis closely follows the study of *Konopka et al.* [2009]. The main novelties are the explicit inclusion of horizontal in-mixing, whereas *Konopka et al.* [2009] simply argued for in-mixing which was not included in their analysis to close the ozone budget, the inclusion of further tracers (H_2O and CO) and a thorough treatment of the sensitivities of the results. Throughout this work, we use potential temperature as the vertical coordinate, because *Konopka et al.* [2009] showed that on constant pressure surfaces the annual ozone cycle appears considerably larger due to the relative movement of pressure and potential temperature surfaces.

[11] In section 2 the back trajectory method is introduced. Section 3 presents the results, concerning the impact of in-mixing on the TTL tracer seasonality. Section 4 shows a sensitivity analysis with respect to the strength of tropical upwelling. We summarize and conclude in section 5.

2. Backtrajectory Method

[12] To separate the effect of horizontal in-mixing from the effect of vertical upwelling on the seasonality of the TTL tracer composition, we reconstruct mean TTL mixing ratios using 3D back trajectories. For this purpose, five-month diabatic [e.g., *Schoeberl et al.*, 2003] back trajectories are started on a $2^\circ \times 2^\circ$ latitude-longitude grid on the 370, 380, 390, 400, 410, 420, 430, 440, 450 K isentropes between 30°S–30°N latitude, on the 15th of each month for the years 2004–2005. For the trajectory calculation we use the CLaMS trajectory module [*McKenna et al.*, 2002] and meteorological fields from the European Centre for Medium-range Weather Forecasts (ECMWF) ERA-Interim reanalysis [*Simmons et al.*, 2006; *Uppala et al.*, 2008]. The trajectories are calculated using potential temperature θ as the vertical coordinate, with the (diabatic) vertical velocity deduced from the forecast total diabatic heating rate [cf. *Fueglistaler et al.*, 2009b; *Ploeger et al.*, 2010].

[13] The back trajectories are initialized at their end points (earliest date, five months before launch) with water vapor, and at the first time when they reach below 360 K with ozone and carbon monoxide mixing ratios from Microwave Limb Sounder (MLS) observations. For the initialization, a latitude-, longitude- and potential temperature dependent monthly mean climatology for the period 2004–2005 is used. Along each trajectory, the water vapor mixing ratio is calculated assuming freeze-drying at 130% relative humidity (yielding best agreement with observations) and instantaneous dehydration [e.g., *Fueglistaler et al.*, 2004; *James et al.*, 2008]. The ozone calculation is based on production due to oxygen photolysis and HO_X-induced chemical loss, as discussed by *Ploeger et al.* [2011]. The carbon monoxide calculation is based on chemical loss due to the presence of OH [*Pommrich et al.*, 2011]. The lower model boundary 360 K for ozone and CO is chosen to avoid modeling tropospheric chemistry.

[14] We separate the effects of horizontal in-mixing from the Northern/Southern hemispheres (NH/SH) and tropical upwelling on mean mixing ratios in the TTL (mean value between 20°S–20°N equivalent latitude, in the following), by

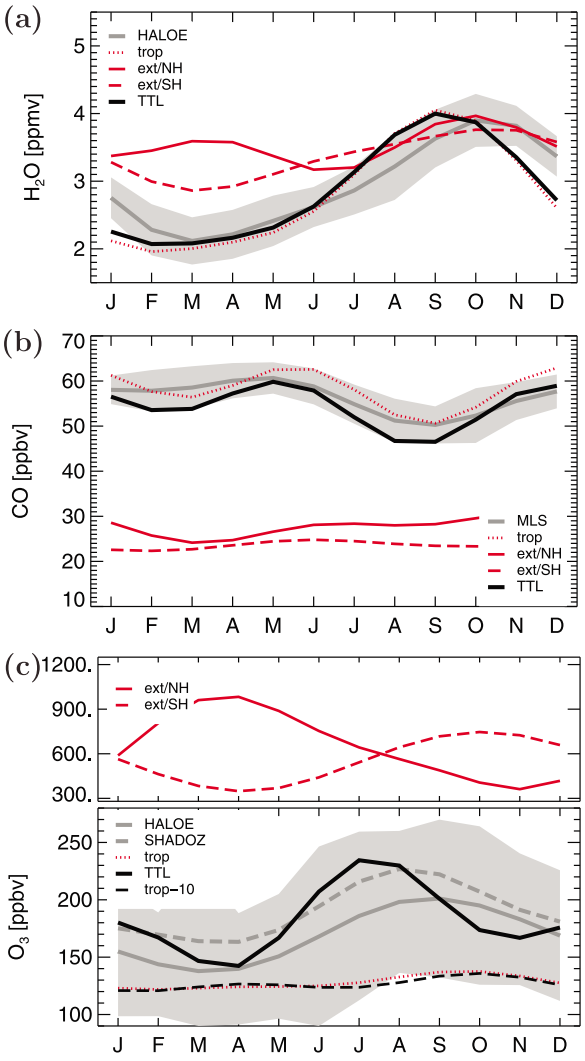

Figure 1. Seasonality of tropical (20°S–20°N equivalent latitude) (a) H_2O, (b) CO and (c) O_3 at 400 K, as 2004–2005 climatology. The gray solid line shows HALOE (MLS for CO) observations (gray shading denoting one standard deviation range), the gray dashed line SHADOZ (only for ozone). The thick black solid line shows mean mixing ratios reconstructed from all back trajectories, the red dotted line only from tropical, the red solid/dashed only from NH/SH in-mixed back trajectories. The black dashed line (for ozone only) shows the mean mixing ratio for trajectories remaining in the deep tropics (10°S–10°N) throughout the integration period. All lines are harmonic fits to the monthly values, using annual and semi-annual harmonics.

dividing the ensemble of back trajectories initialized in this equivalent latitude range into three subensembles. The NH and SH in-mixed sub ensembles are defined as those trajectories which travel through regions polewards ±50° equivalent latitude for at least five days. The remainder defines the tropical sub ensemble. This particular choice for the boundary between tropics and extratropics is motivated by the effective diffusivity analysis of *Haynes and Shuckburgh* [2000], who argue that the tropopause during NH summer is located around ±50° equivalent latitude (at about 350 K). Hence, selecting a threshold latitude of ±50° is a conservative limit, and trajectories defined as in-mixed are very likely of midlatitude origin, representing extratropical air masses. Note that defining the in-mixed ensembles as those back trajectories ending polewards ±50° equivalent latitude (after both three and five months integration time) or choosing different boundary values (30°, 40°), or latitude instead of equivalent latitude, causes no significant change of our conclusions. Also using kinematic back trajectories [e.g., *Schoeberl et al.*, 2003; *Ploeger et al.*, 2010] yields qualitatively the same results.

[15] According to the definitions in the previous paragraph, the mean TTL mixing ratio χ for a particular species can be written as

$$\chi = f_t\chi_t + f_n\chi_n + f_s\chi_s, \quad (1)$$

with χ_n, χ_s and χ_t the mean mixing ratios for the NH in-mixed, the SH in-mixed and the tropical ensembles, respectively. The f's denote the corresponding trajectory fractions, with $f_t + f_n + f_s = 1$. Consequently, the seasonality of tropical mean mixing ratios results from the superposition of the seasonality of the strengths of the different transport pathways (f's) and the respective concentrations (χ's).

[16] Strictly, the ozone mixing ratio of in-mixed back trajectories is not exactly equal to the extratropical initialization value but is affected also by photochemical production along the trajectory. However, the relative contribution of photochemical production to the ozone mixing ratio of an in-mixed trajectory is rather small (e.g., photochemical production changes the mean ozone value of August 2005 NH in-mixed trajectories (555 ppbv) by only about 2% to 568 ppbv).

3. Effect of In-Mixing on O_3, CO and H_2O

[17] Figure 1a shows the climatological (2004–2005) seasonality of tropical mean water vapor at 400 K observed by HALOE (Halogen Occultation Experiment) [*Russell et al.*, 1993] as a gray solid line (one standard deviation range as gray shading) and the back trajectory reconstruction (black solid). The 2004–2005 HALOE climatology is constructed analogously to the climatology of *Grooß and Russell* [2005]. The agreement of the absolute values and the annual cycle amplitudes between both observation and reconstruction is good, but the reconstructed maximum appears about one month too early, consistent with too fast tropical diabatic upwelling in the ERA-Interim data (see section 4). The red solid/dashed lines show the mean mixing ratios of the NH in-mixed and SH in-mixed trajectory ensembles respectively (χ_n and χ_s in the notation of equation (1)), the red dotted line shows the mixing ratio of the tropical ensemble (χ_t). Obviously, the mean TTL mixing ratio (black solid) almost equals the tropical ensemble mixing ratio without in-mixing effects included (red dotted). Therefore, the seasonality of water vapor in the TTL can be understood simply from tropical processes with a negligible effect of in-mixing from midlatitudes.

[18] MLS observations show an annual cycle in the upper TTL also for carbon monoxide (Figure 1b), but in this case with minimum mixing ratios during NH summer/early autumn. The back trajectory calculation reconstructs the

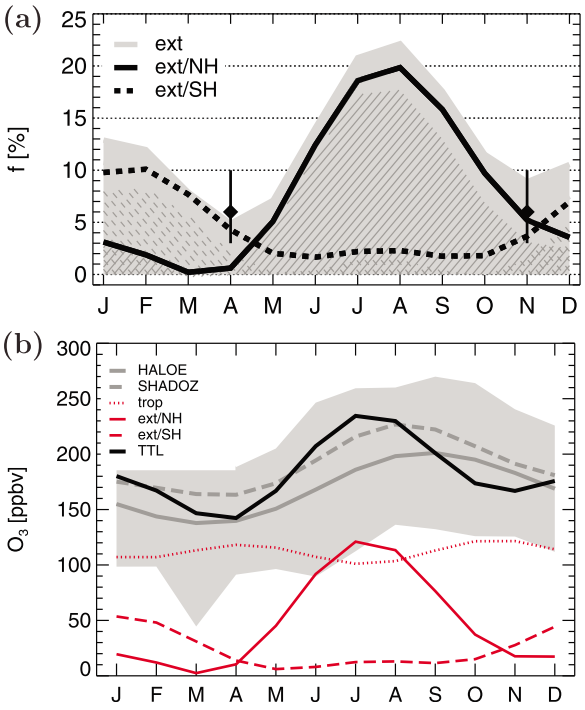

Figure 2. (a) Seasonality (2004–2005 climatology) of horizontal transport into the TTL (in-mixing), diagnosed as fractions of back trajectories (started at 400 K, 20°S–20°N equivalent latitude) traveling polewards 50° equivalent latitude for at least 5 days (gray shaded). The fractions transported from the NH/SH are shown as black solid/dashed lines. The regions hatched with gray solid/dashed lines show the NH/SH fractions for those back trajectories started in the deep tropics between 10°S–10°N equivalent latitude. Black diamonds show the estimate of *Volk et al.* [1996] for comparison. (b) Seasonality of ozone similar to Figure 1c, but for the tropical/NH/SH contributions (red dotted/solid/dashed) to the mean TTL mixing ratio (black solid). All lines are harmonic fits (annual and semi-annual) to the monthly values.

tropical CO seasonality well, with a slightly stronger semi-annual component compared to the observations, causing a second local minimum during February and March. This second minimum is, again, likely related to excessive upwelling in ERA-Interim. MLS observations in the lower TTL around 150 hPa show a semi-annual rather than an annual cycle [*Randel et al.*, 2007, Figure 8], albeit this structure should not be overemphasized, as the MLS CO retrieval has a relatively low vertical resolution. The stronger the upwelling the more clearly the semi-annual signal is detected higher up. For slower upwelling the semi-annual signal is destroyed by chemical loss and in-mixing.

[19] The CO seasonality in the upper TTL is similar to the seasonality of purely tropical transport (red dotted), reconstructed only from the tropical trajectory ensemble. But the agreement is not as close as in the case of water vapor. The NH in-mixed and SH in-mixed air, on the other hand, shows much lower mixing ratios (red solid and dashed). Obviously, the (weak) effect of in-mixing is to lower the tropical mixing ratios, in particular during NH summer when the difference between the pure tropical (red dotted) and the mean TTL mixing ratios (black solid) is largest.

[20] In the case of ozone (Figure 1c), HALOE and SHADOZ (Southern Hemisphere Additional Ozone sonde network) [*Thompson et al.*, 2007] observations (gray solid and dashed) as well as the reconstruction all show the annual cycle discussed in *Randel et al.* [2007] and *Konopka et al.* [2009], with maximum during NH summer and minimum during winter. For SHADOZ, we use the tropical mean climatology of *Randel et al.* [2007], based on a subset of seven stations and the period 1998–2006. There is a large variability of tropical mixing ratios around the mean, illustrated by the wide HALOE standard deviation range (gray shading). Moreover, the sensitivity of reconstructed ozone to transport uncertainties in the TTL is rather large, as discussed by *Ploeger et al.* [2011]. Under these conditions, the agreement between the conceptual back trajectory approach and the observations in Figure 1c is encouraging.

[21] The ozone mixing ratio reconstructed from only tropical transport (red dotted), does not show an annual cycle. If we confine tropical transport closer to the equator and consider only trajectories not leaving the 10°S–10°N equivalent latitude range, the reconstruction even reveals a weak semi-annual cycle (black dashed). The two maxima around the equinoxes are due to the strongest solar insulation in the tropics during these seasons causing strongest photolytical ozone production, as discussed by *Konopka et al.* [2009]. Hence, tropical processes do not explain the annual cycle of upper TTL ozone mixing ratios and in-mixing effects have to be included in the calculation to deduce a realistic ozone seasonality.

[22] Mean mixing ratios for the in-mixed trajectory ensembles are shown in the top panel of Figure 1c. These midlatitude ozone values are five to ten times larger than the tropical mixing ratio. Ozone mixing ratios on the NH show an annual cycle with maximum during February–April when extratropical downwelling on the NH is strongest, and on the SH an annual cycle with maximum during September–November. Therefore, neither tropical transport nor the seasonal cycle of the in-mixed ozone directly reflect the ozone annual cycle in the TTL with its summer maximum.

[23] To understand how the ozone annual cycle in the TTL results from the superposition of tropical and in-mixed ozone mixing ratios, we analyze the strength of horizontal in-mixing, diagnosed from the fraction of in-mixed back trajectories in Figure 2a. In-mixing from the NH and from the SH both clearly show inversely phased annual cycles, with maximum in-mixing during NH summer from the NH (black solid) and during NH winter from the SH (black dashed). The regions hatched with gray solid/dashed lines show the NH/SH in-mixed fractions for back trajectories started between 10°S–10°N. Evidently, the strong in-mixing during NH summer penetrates deeply into the tropics. Due to the stronger seasonality of in-mixing from the NH than from the SH, the superposition of both in-mixing terms approximately yields an annual cycle for total in-mixing from the extratropics, with maximum during NH summer (gray shading).

[24] During NH summer, about 20% of the air in the TTL originates polewards 50° equivalent latitude. The midlatitude air fraction of about 6% (around 400 K) of the study of *Volk et al.* [1996] punctually validates our ECMWF-based results.

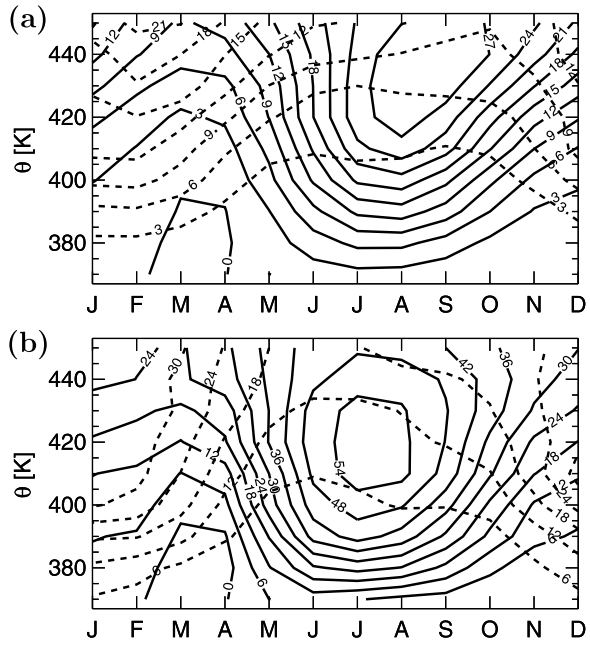

Figure 3. (a) Fractions of in-mixed back trajectories (started between 20°S–20°N equivalent latitude), in-mixed from the NH polewards 50° equivalent latitude (solid contours) and from the SH polewards −50° (dashed) in per cent. (b) In-mixing contributions from the NH (solid) and SH (dashed) to the mean TTL ozone mixing ratio in per cent. All lines are harmonic fits (annual and semi-annual) to the monthly values.

The 6% value (black diamonds) was estimated from tracer in-situ observations during April and October and is in good agreement with the April/October in-mixing fractions of Figure 2a. However, the strong seasonality of in-mixing, with the largest values during NH summer, is not included in the analysis of *Volk et al.* [1996]. We emphasize again that although the diagnosed fraction of in-mixed air depends on the choice of the (equivalent) latitudinal boundary value between tropics and extratropics (e.g., the in-mixed fraction for August varies between 30, 22, 17% for 40°, 50°, 60° boundaries), the distinct seasonality of in-mixing and its impact on trace gases turns out to be largely independent of this particular choice.

[25] The seasonality of mean ozone mixing ratios in the TTL results from the superposition of the purely tropical and the in-mixed concentrations (see Figure 1), weighted with the time-dependent transport fractions of Figure 2a. Figure 2b shows the contributions of the three different pathways to mean TTL ozone (black line), in the notation of equation (1) the terms $f_t\chi_t$, $f_n\chi_n$ and $f_s\chi_s$. The tropical contribution (red dotted) shows a weak semi-annual variation, the SH in-mixed contribution a weak annual cycle with maximum during NH winter and the NH contribution a strong annual cycle with maximum during NH summer. Hence, the summer maximum of TTL ozone can be clearly attributed to in-mixing of ozone-rich air from the NH midlatitudes, with about 55% of TTL ozone (about 130 ppbv) of extratropical origin. Although, neither purely tropical nor in-mixed ozone values exhibit the correct seasonality, the strong peak in the intensity of in-mixing in NH summer causes the summer maximum in mean TTL mixing ratios.

[26] Note that the maximum fraction of in-mixed air during NH summer is only about 20% (Figure 2a). Therefore, the impact of in-mixing on the mean TTL mixing ratio largely depends on the horizontal gradient of the considered species. A simple back of the envelope calculation illustrates this point. From Figure 1 we deduce a mean TTL ozone mixing ratio for July of about 230 ppbv and a mean NH in-mixed mixing ratio of about 650 ppbv. Hence, 20% of in-mixed air causes a contribution of about 130ppbv (about 55%) to mean TTL ozone. For CO on the contrary, the mean TTL and NH in-mixed values for August are about 50 ppbv and 30 ppbv, and in-mixing contributes only about 10% to the mean TTL value.

[27] For the same reason, a classical tracer of stratospheric transport that is well conserved in the lower stratosphere, N_2O, cannot constrain lateral in-mixing. Typical N_2O mixing ratios in the tropical upper troposphere are about 320 ppbv, in the NH lower stratosphere about 310 ppbv [*Homan et al.*, 2010]. Hence, in-mixing of 20% extratropical air would change the tropical mixing ratio by less than one percent, a value hardly detectable by currently available observations.

[28] Figure 3a presents the vertical dependence of the fraction of in-mixed air diagnosed from the in-mixed back trajectories. During NH summer, the TTL composition shows a non-vanishing fraction of air from the NH extratropics above about 370 K, increasing with height throughout the TTL. The contribution of extratropical ozone to the mean TTL ozone mixing ratio in Figure 3b mirrors the in-mixed air contours. While the NH extratropical contribution to ozone at about 370 K is only about 5% in NH summer, it increases strongly with height to about 50% above 400 K. Remarkably, the contribution of in-mixed ozone to the TTL mixing ratio (Figure 3b) is about twice as large as the fraction of in-mixed trajectories (Figure 3a).

[29] To investigate the cause of horizontal in-mixing into the tropics, Figure 4 shows the probability distribution for the locations of in-mixing from the NH/SH (top/bottom part of each panel) of back trajectories in the meridional plane across 50° equivalent latitude, during NH summer (Figure 4a) and winter (Figure 4b). The black contours show the mean summer (jja) and winter (djf) equatorwards directed meridional winds, for 2004–2005, averaged between 20° and 50° equivalent latitude. During NH summer (Figure 4a), main in-mixing occurs from the NH between about 80° and 200° and around 300° longitude, between about 370 and 420 K, at locations, where the anticyclonic flow of the Asian and the North American ('Mexican') monsoons is directed toward the equator (compare the meridional wind contours). Similarly, during NH winter (Figure 4b), maximum in-mixing occurs from the SH around 220° and 320° longitude, in the outflow regions of the Australian and the South American ('Bolivian high') monsoons. Daily maps of trajectory positions (not shown) demonstrate that in-mixed trajectories indeed follow the anticyclonic monsoon flow from high latitudes and enter the TTL on the eastern side of the anticyclone. Thus, the monsoons, in particular the Asian monsoon, turn out to be the main driving factors for in-mixing from the extratropics into the TTL. Note, that a strong impact of the Asian monsoon on

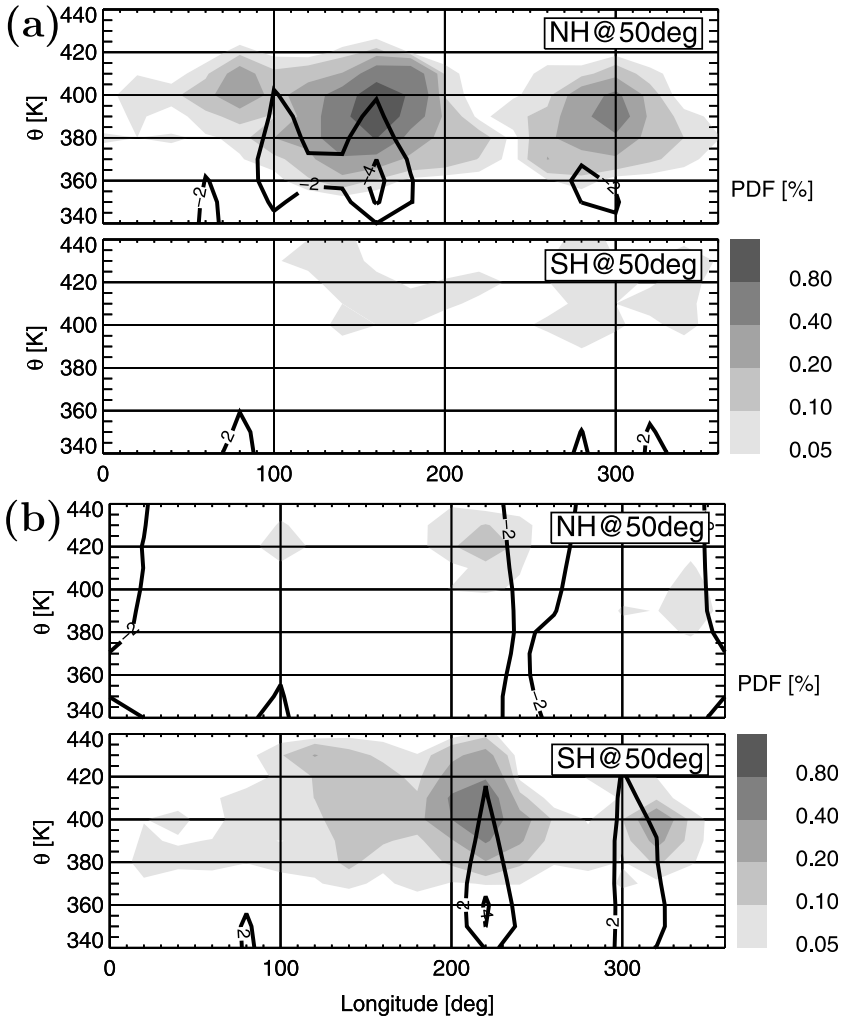

Figure 4. (a) PDFs of locations of horizontal transport (in-mixing) across 50° equivalent latitude into the tropics for back trajectories, started between 370 K and 450 K on 15 August 2005. (b) Same as Figure 4a, but for starting date 15 February 2005. The black lines are 2004–2005 climatological summer (jja) and winter (djf) meridional wind contours, averaged between 20° and 50° equivalent latitude (NH: −2, −4 m/s; SH: 2, 4 m/s).

in-mixing was already proposed by *Dunkerton* [1995], *Chen* [1995] and *Konopka et al.* [2010].

4. Sensitivity Analysis for In-Mixing and Upwelling

[30] Uncertainties in transport in the TTL and lower stratosphere may affect our results based on trajectory calculations. To test whether our conclusions regarding in-mixing of extratropical air are robust, we formulate a complementary 1D model of the chemical composition of the TTL in section 4.1. The 1D model will be driven by the mean tropical vertical velocity and in-mixing rates and will be used to analyze the sensitivity of our conclusions with respect to the strength of in-mixing and upwelling.

[31] First, we deduce the range of the tropical vertical upwelling velocity in the upper TTL consistent with atmospheric observations by performing a radiative heating rate calculation (for clear-sky conditions), using the Edwards-Slingo radiation code [*Edwards and Slingo*, 1996; *Walters et al.*, 2011]. The main factors determining tropical heating rates are temperature, water vapor and ozone. We estimate the range of tropical temperatures, entering the radiative calculation, from GPS radio occultation data from CHAMP (CHAllenging Minisatellite Payload), which is described by *Schmidt et al.* [2004, 2010]. Therefore, we use observed monthly mean climatological (2001–2008) tropical average temperatures (10°S–10°N) plus and minus one standard deviation. The range of tropical ozone and water vapor is estimated from HALOE climatological (1991–2002) observations [*Grooß and Russell*, 2005]. Three different profiles result for each of the three species, the climatological mean and the mean plus and minus one standard deviation. For each month, a heating rate profile is calculated for each of the 27 possible combinations. We assume that the ensemble of these profiles covers the range of variability of possible states of the tropical atmosphere, relevant for tropical heating rates.

[32] Figure 5a shows the radiatively calculated seasonality of the tropical diabatic vertical velocity $\dot{\theta}$ at about 85 hPa, and

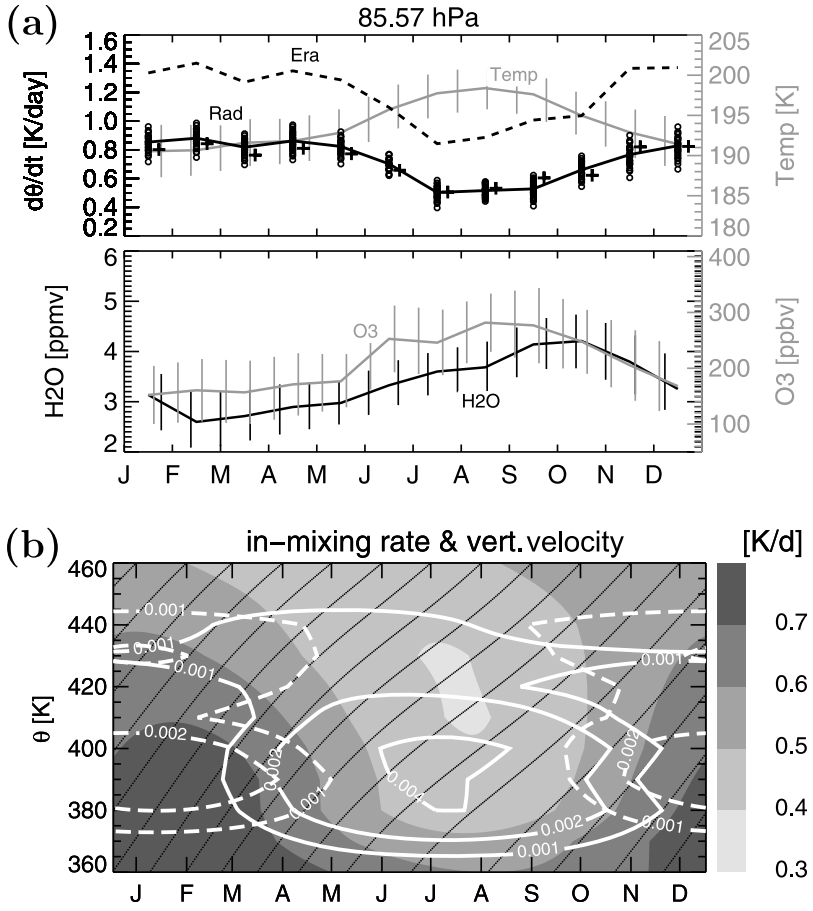

Figure 5. (a) Seasonality (top) of tropical (diabatic) vertical velocity $\dot{\theta}$ at 85 hPa from a radiative heating rate calculation (denoted 'Rad') and for temperatures from CHAMP (light gray y axis), and (bottom) for H_2O and O_3 from HALOE. ERA-Interim clear-sky radiative heating rate velocity as black dashed line ('Era'), and multiplied by 0.6 (crosses). The black circles show the vertical velocity variability estimated from the temperature, O_3 and H_2O variability in the CHAMP/HALOE data. (b) Tropical (diabatic) vertical velocity $\dot{\theta}$ in K/day as 2004–2005 climatology from ERA-Interim multiplied by 0.6 (gray shading) and in-mixing rates from NH (white solid lines) and SH (white dashed) extratropics in day^{-1} (see text for details; contour scaling 0.001, 0.002, 0.004 d^{-1}). Velocities and in-mixing rates are fitted with annual harmonics. Black lines show 1D back trajectories started at 460 K.

the input data for the calculation. The gray line in Figure 5a (top) shows the CHAMP observed mean temperature, with the error bars representing the range of plus and minus one standard deviation. The gray and black lines in Figure 5a (bottom) display the mean and variability of HALOE ozone and water vapor. The black open circles (Figure 5a, top) show the 27 different $\dot{\theta}$ values, the range of vertical velocity, for each month. The black solid line shows the mean, which is interpreted as the most likely value, and which is in good agreement with other heating rate estimates [e.g., *Randel et al.*, 2007; *Fueglistaler et al.*, 2009b].

[33] The seasonal cycle of tropical vertical velocities with maximum upwelling during NH winter and minimum upwelling during NH summer, in phase opposition with the temperature cycle, is clearly evident. ERA-Interim diabatic vertical velocity for clear-sky conditions (dashed line in Figure 5a, top) shows substantially greater values by 0.4–0.6 K/d (for a discussion of heating rate differences, see *Fueglistaler et al.* [2009b]. ERA-Interim overestimates both the annual mean and the annual amplitude values, such that a simple correction factor of 0.6 for the ERA-Interim $\dot{\theta}$ (black crosses) yields good agreement with our radiative calculation, not only at 85 hPa but in the whole layer between 150–70 hPa (not shown). This overestimation of the tropical upwelling velocity is in good agreement with *Dee et al.* [2011], where it was noted that the water vapor upward transport throughout the TTL and lower stratosphere in ERA-Interim is almost twice as fast as indicated by observations.

[34] The annual cycle is defined here as the first harmonic approximation, i.e., by two parameters, the annual mean and the annual amplitude. Consequently, the variability of $\dot{\theta}$ values from the radiative calculation translates into the variability of these parameters. Thus, the radiative calculation restricts the range of the annual mean tropical upwelling at 85 hPa to $0.61 \leq \langle \dot{\theta} \rangle \leq 0.83$ K/d and the range of the amplitude of the annual cycle in upwelling to $0.08 \leq \dot{\theta}_a \leq 0.27$ K/d

(in the following, square brackets denote the annual mean, the subscript 'a' the annual amplitude). These values translate into a range of correction factors for ERA-Interim mean upwelling ($\langle\dot{\theta}^{\mathrm{ERA}}\rangle = 1.19\mathrm{K/d}, \dot{\theta}_a^{\mathrm{ERA}} = 0.28\mathrm{K/d}$), such that $0.5 \cdot \langle\dot{\theta}^{\mathrm{ERA}}\rangle \le \langle\dot{\theta}\rangle \le 0.7 \cdot \langle\dot{\theta}^{\mathrm{ERA}}\rangle$, and for the ERA-Interim annual upwelling amplitude $0.3 \cdot \dot{\theta}_a^{\mathrm{ERA}} \le \dot{\theta}_a \le 1 \cdot \dot{\theta}_a^{\mathrm{ERA}}$.

4.1. Tropical 1D Model

[35] To study the robustness of the results from the previous section 3 and to further analyze the in-mixing into the tropics, we use a simple 1D model for the time- and potential temperature-dependent tracer mixing ratio $\chi(t, \theta)$ in the TTL

$$\partial_t\chi + \dot{\theta}\,\partial_\theta\chi = P - L\chi - \alpha^n(\chi - \chi_n) - \alpha^s(\chi - \chi_s). \quad (2)$$

Here, P is the chemical production rate and L the chemical loss rate. The last two terms on the right-hand side of equation (2) represent horizontal in-mixing into the tropics from the NH (n) and the SH (s) as a linear relaxation to mean midlatitude values χ_n and χ_s [cf. *Volk et al.*, 1996]. The functions P, L, α^n and α^s may depend on potential temperature and time, the χ_i depend only on potential temperature (defining the χ_i to depend also on time causes no significant change of our results). The 1D model is similar to the model of *Volk et al.* [1996], with the main difference that we assume the entrainment (or in-mixing) rates α^n and α^s to be time-dependent. This assumption is necessary due to our finding of the strong seasonality in the fraction of in-mixed extratropical air in section 3.

[36] To solve equation (2) for the mixing ratio χ we consider the 1D motion of air parcels rising in the tropics, termed 1D tropical trajectories in the following. Along these trajectories $\partial_t + \dot{\theta}\,\partial_\theta = \frac{\mathrm{d}}{\mathrm{d}t} = \dot{\theta}\frac{\mathrm{d}}{\mathrm{d}\theta}$ and equation (2) can be written

$$\frac{\mathrm{d}\chi}{\mathrm{d}\theta} = -\gamma\chi + \frac{P + \alpha^i\chi_i}{\dot{\theta}}, \quad (3)$$

with $\gamma = \frac{L+\alpha^n+\alpha^s}{\dot{\theta}}$. Here and in the following, a summation over the index $i \in \{n, s\}$ is understood to simplify the notation, such that $\alpha^i\chi_i = \alpha^n\chi_n + \alpha^s\chi_s$. The first term on the right-hand side causes destruction of tracer mixing ratio due to chemical loss and dilution from in-mixing of extratropical air. The second term is a production term, including production due to both photochemistry and in-mixing. The mixing ratio χ is then calculated by integrating the various source terms on the right-hand side of equation (3) along the tropical trajectories.

[37] It is important to note that both forcings due to chemical production and in-mixing on the right-hand side of equation (3) appear with the same denominator $\dot{\theta}$. As a consequence, slower upwelling causes stronger production of mixing ratio due to longer ascent times for both photochemical production and for in-mixing of extratropical air, such that the ratio of chemically produced and in-mixed tracer amount remains constant. In other words, for each thin θ-layer the amount of in-mixed relative to the amount of photochemically produced tracer mixing ratio,

$$\frac{\chi^{\text{in-mixed}}}{\chi^{\text{chem}}} = \frac{\alpha^i\chi_i}{P}, \quad (4)$$

is independent of the upwelling velocity $\dot{\theta}$. As this relation holds for each thin θ-layer, it holds throughout the tropics. An analytic solution of equation (3) for χ can also be written down, given by equation (A1) in Appendix A, and confirms this finding.

[38] Note, that we have neglected vertical diffusion in equation (2). There is no indication for a distinct seasonality in the vertical diffusivity of the tropical atmosphere, neither from observations [*Legras et al.*, 2003, 2005] nor from vertical dispersion of the 3D back trajectories (not shown), which could serve as another forcing of mixing ratio seasonality. A potential effect of a constant diffusivity on the mean TTL mixing ratio and its annual anomaly is a limitation to our analysis and could serve to reconcile slight inconsistencies between our 1D model results and observations, as discussed below. Our results concerning the relative contribution of in-mixing to the TTL mixing ratio, however, are not affected by the neglect of diffusion.

[39] The lower boundary for the model is taken at 360 K potential temperature, and mixing ratios below as well as the mean midlatitude values χ_i are prescribed from a SHADOZ/MLS climatology for O_3/CO. Ozone chemistry is represented as production, with the production rate P the tropical average (10°S–10°N) of the data used in section 3 [cf. *Konopka et al.*, 2009, Figure 2], and CO chemistry is represented as loss with $L = (4\ \text{month})^{-1}$ [e.g., *Randel et al.*, 2007].

[40] The mean tropical vertical velocity $\dot{\theta}$ for the model is taken from the ERA-Interim total diabatic velocity by averaging between 10°S–10°N latitude. Motivated by the results of our radiative calculation, the 'most likely' (reference) velocity is taken to be the ERA-Interim $\dot{\theta}$ multiplied by a factor 0.6 and is shown in Figure 5b. Hence, tropical mean upwelling in the TTL varies between 0.3 K/d during NH summer and 0.8 K/d during NH winter.

[41] We deduce the rates for in-mixing from the NH and SH from the fractions f_i of the in-mixed 3D back trajectories in section 3 (compare Figure 3a), which are interpreted as the fractions of midlatitude air in the tropics at each θ-level. As a tropical parcel ascents, more and more midlatitude air is in-mixed into the parcel and the midlatitude air fraction increases steadily. Hence, the fraction of midlatitude air at a particular θ-level can be calculated by integrating the in-mixing rates along the ascending trajectory. Inverting this relation yields an equation to deduce the in-mixing rates from the midlatitude air fractions,

$$\alpha^i = (\partial_t + \dot{\theta}\,\partial_\theta)f_i. \quad (5)$$

The NH and SH in-mixing rates α^n and α^s are shown as white solid and dashed contours in Figure 5b. Maximum in-mixing from the NH occurs during NH summer between 380–420 K and from the SH during NH winter, with NH in-mixing significantly stronger than SH in-mixing. Strictly speaking, the in-mixing rates calculated via equation (5) depend on the meteorological data, in particular on the vertical velocity, used for the 3D back trajectory calculation. However, the tropical upwelling velocity $\dot{\theta}$ and the horizontal in-mixing rates α^i are caused by very different atmospheric processes, the Brewer-Dobson circulation (for $\dot{\theta}$) and the monsoon circulations (for α^i). Therefore, we assume $\dot{\theta}$ and α^i to be

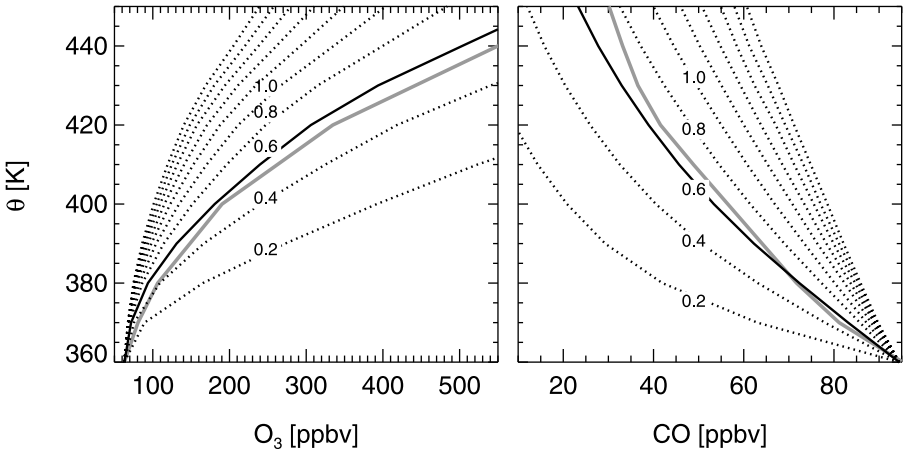

Figure 6. Sensitivity to mean tropical upwelling of annual mean tropical (10°S–10°N latitude) (left) O_3 and (right) CO profiles from the tropical 1D model. Numbers denote multiplication factors for ERA-Interim mean upwelling (spacing 0.2, see text). The gray lines show SHADOZ (for O_3) and MLS (CO) observed profiles.

independent of each other in leading order. Following this line of argument, the vertical velocity dependence in equation (5) is not solely due to the explicit $\dot{\theta}$ but also due to an implicit dependence of the midlatitude air fractions f_i (slower upwelling causes in-mixing of midlatitude air into ascending tropical air parcels over longer times and hence larger f_i's), which are likely to cancel leaving the α^i independent of $\dot{\theta}$. Here, we simply assume independence of upwelling and in-mixing rates and vary both independently in our sensitivity study (this could be a limitation to our analysis).

[42] Moreover, the annual mean total in-mixing rate (sum of NH and SH in-mixing, $\alpha = \alpha^n + \alpha^s$) for the 370–420 K layer yields an in-mixing timescale of 12.7 months, very similar to the entrainment timescale reported by *Volk et al.* [1996] of about 13.5 months which was derived from in-situ observations assuming time-independent in-mixing. Therefore, we define the reference, or 'most likely', atmospheric state for our 1D model as given by ERA-Interim upwelling multiplied by 0.6 and the back trajectory based ERA-Interim in-mixing rates, as illustrated in Figure 5b.

[43] For use in the 1D model, the mean tropical vertical velocity and the in-mixing rates are fitted with annual harmonics

$$\dot{\theta} = \langle \dot{\theta} \rangle + \dot{\theta}_a \cos(\omega t), \tag{6}$$

$$\alpha^i = \langle \alpha^i \rangle \mp \alpha^i_a \cos(\omega t), \tag{7}$$

at each θ-level, with the minus/plus sign for NH/SH in-mixing, respectively (Figure 5b shows the fitted data). The idealized phases in equation (6) are a minor restriction and using the correct ERA-Interim phases causes no significant change of our results. In the following, the annual mean and the annual amplitude of both upwelling and in-mixing rates will be varied independently to study the response of the tropical mixing ratio. To restrict the number of free parameters in the sensitivity study, we assume a fixed ratio between the NH and SH in-mixing rates. The amplitude and mean of the vertical velocity will be varied throughout the range of values consistent with the radiative calculation, as defined above ($0.5 \cdot \langle \dot{\theta}^{\mathrm{ERA}} \rangle \le \langle \dot{\theta} \rangle \le 0.7 \cdot \langle \dot{\theta}^{\mathrm{ERA}} \rangle$, $0.3 \cdot \dot{\theta}_a^{\mathrm{ERA}} \le \dot{\theta}_a \le 1 \cdot \dot{\theta}_a^{\mathrm{ERA}}$). As there are very few observation based estimates of annual mean in-mixing rates (e.g., the $(13.5\ \mathrm{month})^{-1}$ value of *Volk et al.* [1996]) and none for the annual amplitude, we allow a rather wide range for both, with $0 \le \langle \alpha^i \rangle \le 2 \cdot \langle \alpha^i_{\mathrm{ERA}} \rangle$ and $0 \le \alpha^i_a \le 2 \cdot \alpha^i_{a\ \mathrm{ERA}}$.

[44] As a first consistency check, we calculate the annual mean tropical O_3 and CO profiles for different annual mean upwelling velocities (Figure 6). For O_3, the slower the upwelling the steeper the profile due to longer transit times for ozone production and in-mixing. For CO, slower upwelling causes stronger chemical loss and lower values in the upper TTL. For both O_3 and CO the best fit of observed profiles (gray line, SHADOZ/MLS observations for O_3/CO) results for ERA-Interim upwelling multiplied by 0.6, corresponding to a mean upwelling velocity in the upper TTL of about 0.7 K/d.

[45] The mean profile reconstruction provides a further, independent justification for the about 40% too strong upwelling in the TTL for ERA-Interim, in addition to the radiative calculation above. The excessive tropical upwelling of the ERA-Interim model is consistent with the results of *Fueglistaler et al.* [2009b], showing a cooling impact of ERA-Interim assimilation increments in the TTL. The slight discrepancy between the calculated profiles and the observations is likely due to neglecting any vertical diffusive terms in equation (2). Diffusion would act to mix air of different levels above and below and therefore, because of the curvature of the O_3 and CO profiles, would shift both the O_3 and the CO profiles to higher values at each level.

4.2. Annual Amplitude Forcing

[46] Figure 7 shows the sensitivity of the ozone relative annual anomaly $\Delta\chi/\chi = (\chi - \langle\chi\rangle)/\langle\chi\rangle$ at 400 K with respect to varying the upwelling annual amplitude $\dot{\theta}_a$, the annual mean upwelling $\langle \dot{\theta} \rangle$, the in-mixing annual amplitude α^i_a and

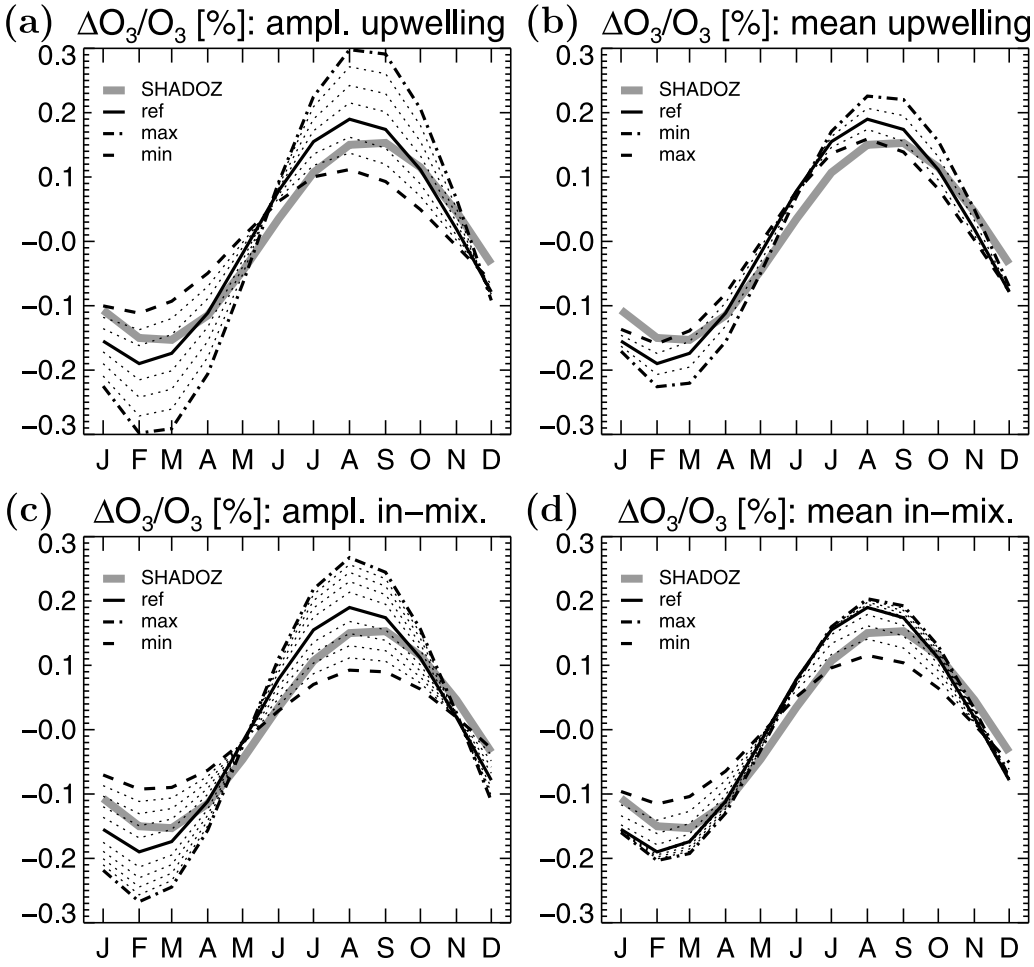

Figure 7. Sensitivity of the relative annual anomaly of tropical (10°S–10°N latitude) ozone $\Delta O_3/O_3$ at 400 K to (a) the seasonality in the upwelling annual amplitude, (b) mean tropical upwelling, (c) the in-mixing annual amplitude, and (d) the mean in-mixing rate, from the 1D tropical model. The black solid line shows the reference case, the dashed/dash-dotted lines the minimum/maximum cases (vice versa for Figure 7b) consistent with the heating rate calculation of Figure 5 (see text). SHADOZ observations are shown as a thick gray line for comparison. Ozone mixing ratios are plotted as the first harmonic approximation.

the annual mean in-mixing rate $\langle \alpha_a^i \rangle$. The black solid lines depict the ozone seasonality for the reference state (ERA-Interim $\dot{\theta}$ multiplied by 0.6 and ERA-Interim in-mixing rates), in good agreement with the SHADOZ observed seasonality (gray).

[47] First, increasing the upwelling annual amplitude $\dot{\theta}_a$ in Figure 7a up to the maximum amplitude case ($\dot{\theta}_a = 1 \cdot \dot{\theta}_a^{\mathrm{ERA}}$, black dash-dotted) causes an increase in the ozone relative annual amplitude, due to longer ascent times allowing more time for photochemical ozone production during NH summer compared to winter. Decreasing the upwelling amplitude to the minimum amplitude case ($\dot{\theta}_a = 0.3 \cdot \dot{\theta}_a^{\mathrm{ERA}}$, black dashed), on the other hand, causes a decrease in the ozone amplitude. Second, an increase in the annual mean upwelling velocity $\langle \dot{\theta} \rangle$ in Figure 7b up to the maximum value (dash-dotted) yields a decrease of the ozone relative amplitude, as the relative difference between summer and winter ascent times decreases.

[48] Third, increasing the in-mixing annual amplitude also increases the ozone annual amplitude (Figure 7c), because the difference between summer and winter in the amount of in-mixed ozone increases. An increase in the annual mean in-mixing rate also weakly increases the ozone annual amplitude.

[49] Evidently, for ozone the sensitivities with respect to the annual amplitudes in upwelling and in-mixing are much greater than with respect to the annual mean upwelling and mean in-mixing rate, and comparable in magnitude. It is worth noting that the annual mean upwelling and in-mixing rates are not representing independent forcings for mixing ratio seasonality. Their effects are non-vanishing only if the annual amplitudes of upwelling or in-mixing rates are non-vanishing.

[50] Consideration of the analytic solution for the annual ozone amplitude equation (A6) in Appendix A shows that the contribution due to the in-mixing amplitude α_a^i is proportional to the annual mean meridional tracer gradient

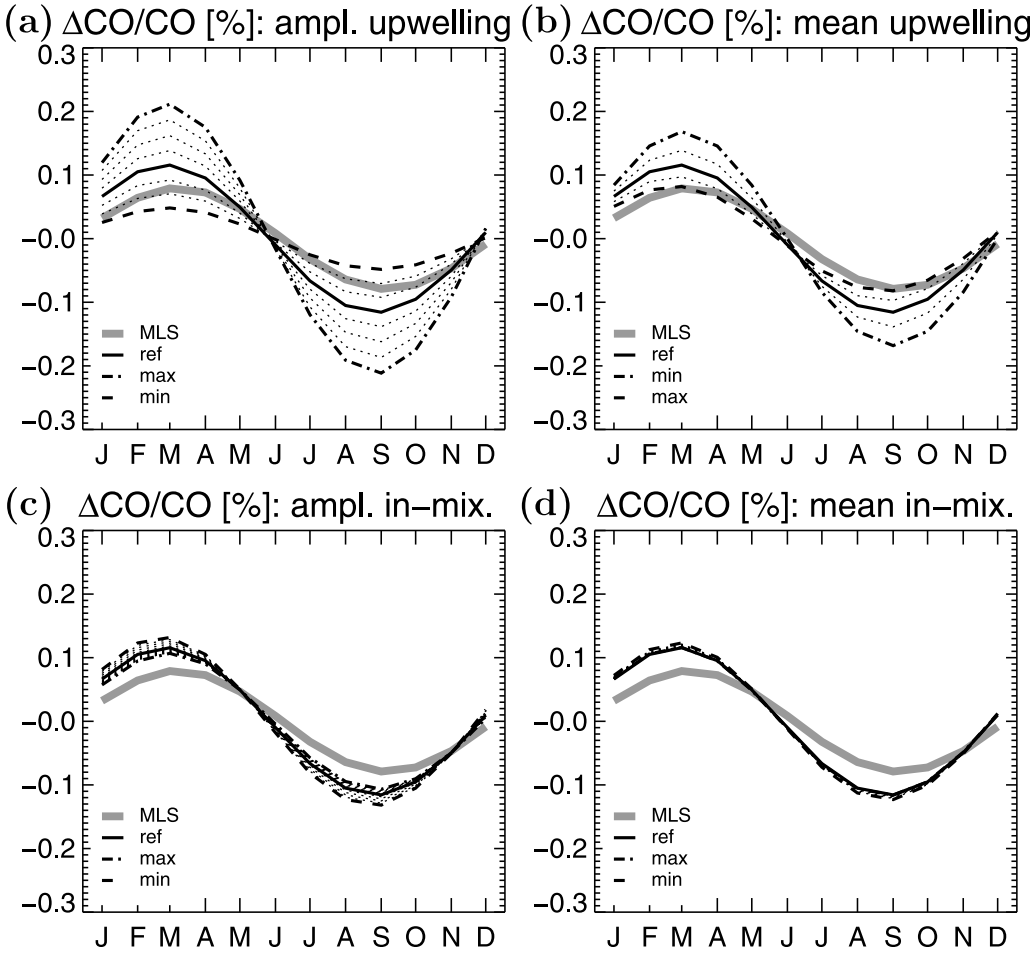

Figure 8. Same as Figure 7 but for CO, and for MLS observations.

($\langle\chi\rangle - \chi_i$) and with respect to the upwelling amplitude $\dot{\theta}_a$ proportional to the mean vertical gradient $\partial_\theta\langle\chi\rangle$. Ozone plays a rather important role as a tracer for in-mixing into the tropics due to the large meridional ozone gradient, with the extratropical ozone mixing ratio about five to ten times larger than the tropical value.

[51] For comparison, the annual cycle amplitude of CO in the tropics (and even more for water vapor) is almost independent of in-mixing of extratropical air (see Figure 8c), as the meridional mixing ratio gradient is too weak. The CO amplitude is forced mainly by the annual amplitude in tropical upwelling, with slower upwelling during NH summer causing longer ascent times for chemical loss and lower CO mixing ratios (Figure 8a). The sensitivity of CO to the transport timescale was recently discussed by *Hoor et al.* [2010] in a different context.

[52] The altitude dependence of the ozone relative annual anomaly $\Delta\chi/\chi$ from SHADOZ observations is presented in Figure 9a, and from the 1D model (reference simulation) in Figure 9b. Evident is the annual cycle in the upper TTL above about 380 K with the anomaly maximum of 15–20% during NH summer and autumn. Above the TTL, the annual cycle amplitude decreases. The modeled ozone even shows a transition from an annual to a semi-annual variation above about 450 K, with two maxima around May and November.

[53] Figure 9c shows the relative annual anomaly for the in-mixed ozone contribution only, $\Delta\chi^{\text{in-mixed}}/\chi$ (with $\Delta\chi^{\text{in-mixed}} = \chi^{\text{in-mixed}} - \langle\chi^{\text{in-mixed}}\rangle$), deduced from the difference between the 1D model calculation with and without in-mixing. The annual cycle in the upper TTL can be clearly attributed to in-mixed ozone, which dominates the seasonal variations up to about 430 K. The semi-annual variation above (compare Figure 9b) is not evident in the in-mixed ozone and therefore results from photolytical ozone production in the tropics.

[54] The tilt of the percentage contours indicates an upward propagation of the summer maximum for the in-mixed ozone contribution (Figure 9c). The fact that there is no distinct tape-recorder signal in mean ozone mixing ratios throughout the tropics (Figures 9a and 9b) is due to the strong increase in photochemical ozone production with height, such that the photochemically produced contribution starts dominating the in-mixed contribution above about 430 K. This explanation for the absence of an ozone tape-recorder is, however, different to the discussion of *Schoeberl et al.* [2008]. *Schoeberl et al.* [2008] conclude that for ozone the seasonal variations in the tropics are forced by the seasonally varying mean flow acting on the strong background ozone gradient, a mechanism which cannot induce a tape recorder behavior. Following our explanation, seasonally varying in-mixing of

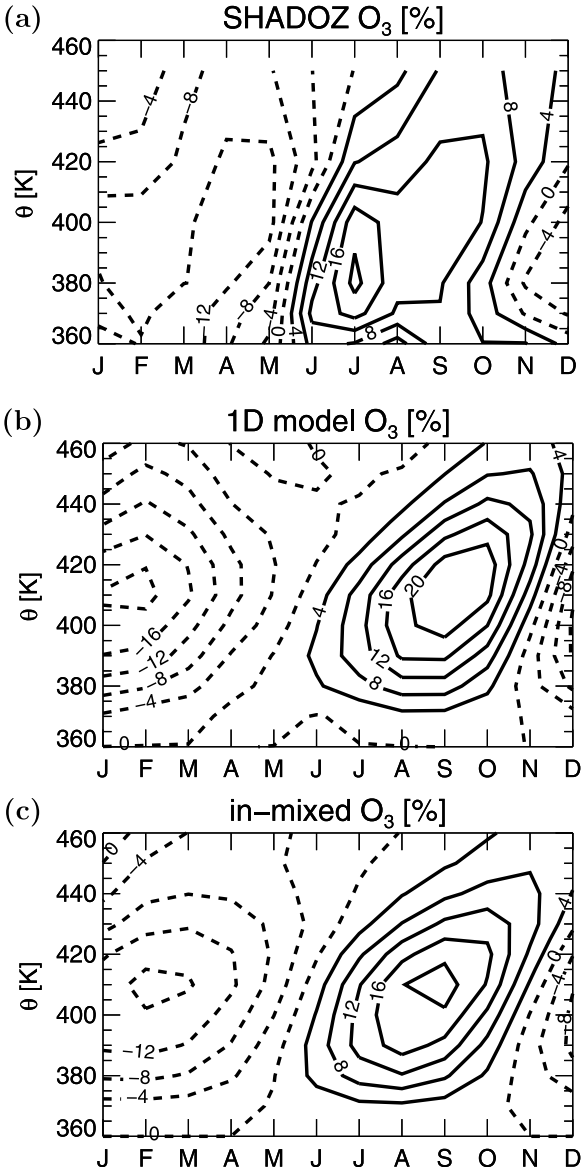

Figure 9. (a) Relative annual anomaly for tropical ozone from the SHADOZ observations. (b) Same as Figure 9a but for ozone from the 1D model reference simulation. (c) Same as Figure 9a but for the in-mixed ozone contribution only (calculated from the difference between 1D model runs with and without in-mixing).

ozone-rich extratropical air into the tropics and subsequent tropical ascent would cause an ozone tape-recorder. The tropical tracer balance equation (2) allows for this in-mixing related tape-recorder, as we discuss in Appendix A below equation (A7). However, in the case of ozone the fast photochemistry effaces the signal already directly above the TTL.

4.3. In-Mixing Contribution for O_3

[55] In the following, we study the robustness of the in-mixed ozone contribution with respect to the upwelling strength, hence to the quality of the ECMWF vertical velocity (deduced from the diabatic heating budget).

[56] For the reference simulation, in-mixed ozone contributes about 40% to the maximum of the TTL ozone mixing ratio during NH summer (calculated as $\chi^{\text{in-mixed}}/\chi$). The impact of in-mixed midlatitude air on the seasonality of mean TTL ozone becomes even more clear by subtracting the annual mean ozone background value. Doing so, we calculate the contribution of the annual amplitude of in-mixed ozone to the TTL ozone annual amplitude as $\chi_a^{\text{in-mixed}}/\chi_a$. This contribution even amounts to about 90%. Both values from the 1D model are in good agreement with the 3D back trajectory results of about 50% and 90% above (Figure 2).

[57] Figure 10a shows the contribution of in-mixing to the mean TTL ozone mixing ratio at the summer maximum (calculated as $\chi^{\text{in-mixed}}/\chi$) for different choices of the upwelling annual mean and annual amplitude (x- and y axis values are given in terms of the ERA-Interim velocity). Throughout the range of 'realistic' velocities, consistent with the radiative calculation shown above (dark gray shaded region), the contribution of in-mixing is larger than about 37%. Remarkable is the rather weak dependence of the in-mixing contribution to varying the vertical upwelling velocity, with the in-mixing contribution changing only from 37–46% throughout the 'realistic' velocity range. This

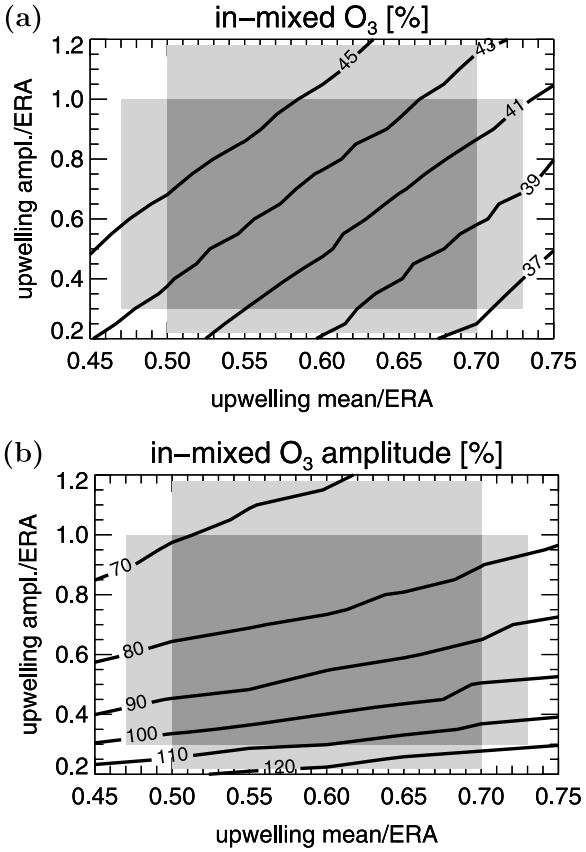

Figure 10. (a) Relative contribution of in-mixing to the ozone summer maximum (calculated from the difference between 1D model reference runs with and without in-mixing) for various choices of upwelling mean (x axis) and upwelling amplitude (y axis). (b) Same as Figure 10a but for the contribution of in-mixing to the ozone annual amplitude. The gray shading shows the range of upwelling mean and amplitude compatible with the radiative calculation of Figure 5.

robustness of the in-mixed contribution is a consequence of equation (4), namely that the amount of in-mixed relative to the amount of photochemically produced tracer mixing ratio is independent of the vertical velocity. Therefore, the relative contribution of in-mixing to mean TTL ozone turns out to be almost independent of the ascent velocity. The slight deviation from this independency in Figure 10a is related to the lower model boundary being at 360 K and the nonvanishing lower boundary ozone value, which is advected upwards with a different $\dot{\theta}$-dependence (compare equation (A1)).

[58] The in-mixed contribution is, however, dependent on the magnitude of the in-mixing rate. An about 20% weaker/stronger in-mixing rate (realized by scaling the ERA-Interim reference value) results in about 5% less/more in-mixed ozone (not shown). As noted above, our reference total in-mixing rate $\alpha = \alpha^n + \alpha^s$ almost equals the estimate of *Volk et al.* [1996] in the annual mean. The in-mixing rate of *Volk et al.* [1996], in turn, was deduced from observations during spring and autumn, both seasons of minimum in-mixing into the tropics (compare Figure 2a and Figure 5b). Therefore, we consider the $(13.5\ \text{month})^{-1}$ value of *Volk et al.* [1996] reduced by 20% as a lower bound for the in-mixing rate and the associated 30% of in-mixed ozone as a lower limit for in-mixed ozone. In summary, both the 1D model and the 3D back trajectory study show evidence for an in-mixing contribution to the ozone summer maximum value of at least 30%, and most likely of about 40–50%, independent of the vertical upwelling velocity.

[59] Because the in-mixed ozone contribution is, by far, largest during NH summer, the contribution of in-mixing to the TTL annual amplitude, calculated as $\chi_a^{\text{in-mixed}}/\chi_a$, is even larger. Throughout the range of 'realistic' velocities this contribution is always larger than 70% (Figure 10b), and larger than about 65% for in-mixing rates reduced by 20%. Consequently, in-mixing of extratropical ozone is the main forcing mechanism for the ozone annual anomaly in the upper TTL, independent of the strength of tropical upwelling. Remarkably, the contribution of in-mixing to the ozone annual amplitude in Figure 10b varies mainly in the y-direction (upwelling amplitude) and is rather independent of the mean upwelling velocity.

5. Summary and Discussion

[60] Three-dimensional back trajectories and a one-dimensional model for tropical trace gas mixing ratios are used to investigate the impact of horizontal in-mixing from the extratropics into the tropics on the trace gas composition of the TTL.

[61] We find that the fraction of in-mixed air shows an approximate annual cycle with maximum values during NH summer, resulting from the superposition of two inversely phased annual cycles for in-mixing from the NH and from the SH. The trajectory motion shows that horizontal in-mixing is mainly driven by the anticyclonic circulations of the large monsoon systems in the subtropical upper troposphere and lower stratosphere. On the one hand, maximum in-mixing from the SH extratropics occurs during NH winter due to the Australian, the South American and the African monsoons. The summer maximum of in-mixing from the NH, on the other hand, can be attributed to the Asian and the North American (Mexican) monsoons. Because the Asian monsoon is the strongest by far, horizontal in-mixing is dominated by in-mixing from the NH with its maximum during NH summer. The net fraction of in-mixed air varies between maximum values around 20% during NH summer and minimum values around 5–10% during spring and autumn.

[62] In general, the seasonal variation of in-mixing turns out to be an important forcing factor for the seasonality of tropical trace gas mixing ratios. However, its impact on the tropical tracer seasonality depends crucially on the lower stratospheric meridional gradients of the considered species. Consequently, the annual cycle of water vapor mixing ratios above the tropical tropopause is largely unaffected by horizontal transport of extratropical air into the tropics, as the difference between extratropical and tropical mixing ratios above the tropopause is small. For the same reason, also for carbon monoxide the impact of in-mixing on the tropical seasonality is weak. But for ozone, a species with extremely large meridional gradients the annual cycle above the tropical tropopause is largely controlled by in-mixing of ozone-rich extratropical air during NH summer.

[63] Three-dimensional back trajectories and a simple one-dimensional tropical model clearly show that, although the fraction of in-mixed air is not particularly large (around 10% in the annual mean), it contributes most likely 40–50% to the ozone summer mixing ratio maximum in the upper TTL (at least about 30% for weak in-mixing). Furthermore, a radiative calculation as well as simulations of mean tropical ozone and carbon monoxide mixing ratios consistently show that the upwelling velocity in the TTL deduced from ERA-Interim diabatic heating rates is about 40% too fast. However, the amount of in-mixed relative to the amount of photochemically produced ozone mixing ratio in the TTL is independent of the vertical ascent velocity, as the effect of slower upwelling is to increase the ozone mixing ratio due to both more photochemically produced and more in-mixed ozone. Hence, almost independently of the strength of tropical upwelling, the ozone annual anomaly in the upper TTL is mainly caused by transport of ozone rich air from midlatitudes into the tropics around the easterly flanks of the Asian and American monsoon anticyclones, with at least about 65% of the ozone annual amplitude related to in-mixing.

[64] The result of about 50% of TTL ozone during NH summer contributed by in-mixing is a statement independent of the vertical coordinate used (here θ). If 50% of the ozone mixing ratio on a certain potential temperature surface is caused by in-mixing, on the corresponding pressure surface (or any other coordinate surface) also 50% of ozone is caused by in-mixing. The ozone annual cycle, on the other hand, changes when the vertical coordinate is changed and it is not obvious how large the in-mixing contribution to the annual amplitude is in pressure coordinates.

[65] Analysis of the Transformed Eulerian Mean (TEM) balance equation for ozone shows that the annual cycle of upwelling acting on the ozone annual mean background gradient provides the main forcing of the ozone annual amplitude on a given log-pressure level [*Randel et al.*, 2007]. As our Lagrangian approach disentangles the effects of tropical vertical transport and horizontal in-mixing, which both affect the mean background gradient, it is not straightforward to compare our findings to these TEM balance based results (see also equation (A5) in Appendix A).

[66] Recently, *Randel et al.* [2007] and *Fueglistaler et al.* [2011] discussed the role of the annual cycle of tropical ozone to partly affect the annual cycle of tropical lower stratospheric temperatures, as a response to radiative effects. *Fueglistaler et al.* [2011] showed evidence for dynamically induced seasonal ozone variations to enhance the annual temperature cycle. They attributed about 30% of the temperature maximum during NH summer to radiative heating associated with the ozone summer maximum, in addition to the extratropical wave forcing via the 'downward control' principle [*Haynes et al.*, 1991; *Yulaeva et al.*, 1994]. Consequently, our results, relating the ozone summer maximum mainly to horizontal in-mixing from the extratropics, link part of the temperature cycle in the tropics to horizontal transport, in particular to the subtropical monsoon circulations. There is some debate, however, about the role of tropical waves for upwelling in the TTL [*Fueglistaler et al.*, 2009a], which could provide a link between upwelling variations and in-mixing.

[67] Our findings of the impact of in-mixing on seasonal variations of tropical trace gases (particularly ozone) highlight the role of horizontal transport between extratropics and tropics for the global climate system. Furthermore, our results emphasize the necessity to correctly represent this horizontal transport, in particular the subtropical monsoon circulations, in models.

Appendix A: Tropical 1D Model—Analytical Arguments

[68] The continuity equation for tropical tracer mixing ratio χ for the 1D motion of an air parcel ascending in the tropics (along a 1D tropical trajectory $\theta(t)$) is given by equation (3). The general solution to this equation, for time- and θ-dependent vertical velocity $\dot{\theta}$, midlatitude mixing ratios χ_i (with $i \in \{n, s\}$), in-mixing rates α^i, loss rate L and production rate P, reads

$$\chi(\theta) = \mathrm{e}^{-\int_{\theta_0}^{\theta} \gamma \, \mathrm{d}\theta'} \int_{\theta_0}^{\theta} \left(\frac{\alpha^i \chi_i + P}{\dot{\theta}} \right) \mathrm{e}^{\int_{\theta_0}^{\theta'} \gamma \, \mathrm{d}\theta''} \mathrm{d}\theta' + \chi_0 \mathrm{e}^{-\int_{\theta_0}^{\theta} \gamma \, \mathrm{d}\theta'}, \tag{A1}$$

with $\gamma = \frac{L+\alpha^n+\alpha^s}{\dot{\theta}}$ defined in section 4.1, $\theta_0 = \theta(t_0) = 360$ K the lower model boundary and $\chi_0 = \chi(\theta_0)$. Note, that the solution for trajectories parameterized in time, $\chi(t)$, can be easily deduced from equation (A1) by substituting $\mathrm{d}\theta = \dot{\theta}\mathrm{d}t$.

[69] The second term on the right-hand side is the mixing ratio at the lower boundary (χ_0) diluted by chemical loss and in-mixing. The first term denotes production of mixing ratio along the trajectory, with the in-mixing rates α^i entering the solution as a 'production' term similar to photochemical production P. For ozone, the magnitude of both 'production' terms is comparable, $P \approx 1 - 3$ ppbv/d $\approx \alpha^i \chi_i$, about one percentage of the mean upper TTL mixing ratio per day (using the tropical ozone production rate given by [*Konopka et al.*, 2009, Figure 2], a mean midlatitude mixing ratio $\chi_i \approx 300 - 1000$ ppbv and the annual mean in-mixing timescale of about 13.5 months, reported by *Volk et al.* [1996]). For CO, for comparison, $\chi_i \approx 30$ ppbv [e.g., *Hoor et al.*, 2010] yields an in–mixing contribution of less than 0.1% per day of the upper TTL value.

[70] To simplify the interpretation of equation (A1), we consider a thin θ-layer between θ_0 and θ, such that L, α^i, χ_i, P and $\dot{\theta}$ can be assumed constant. Under this assumption the exponential factors simplify to $\mathrm{e}^{-\int_{\theta_0}^{\theta} \gamma \, \mathrm{d}\theta'} = \mathrm{e}^{-\gamma(\theta-\theta_0)}$, the remaining integral can be evaluated and equation (A1) can be written

$$\chi(\theta) = \left(\alpha^i \chi_i + P\right) \frac{1}{\gamma\dot{\theta}} \left(1 - \mathrm{e}^{-\gamma(\theta-\theta_0)}\right) + \chi_0 \mathrm{e}^{-\gamma(\theta-\theta_0)}, \tag{A2}$$

which is the solution given by *Homeyer et al.* [2011, equation (2)] generalized by including a chemical production term, however in a different context. Hence, for any thin θ-layer in the tropics, the amount of in-mixed relative to the amount of photochemically produced tracer mixing ratio is $\alpha^i \chi_i / P$, depends only on the in-mixing and production rates and is independent of the upwelling velocity.

[71] An equation for the annual amplitude of χ can be derived following *Randel et al.* [2007] and *Schoeberl et al.* [2008] by linearizing equation (2) around the annual mean state, using $\chi = \langle\chi\rangle + \chi'$ (and analogously for $\dot{\theta}, \alpha^i, P, L$), and expanding the perturbations as $\chi' = \sum_j \chi_j e^{i\omega_j t}$. Generally, the index-set of j includes all possible harmonics (semi-annual, annual, .). Note, that neglecting the non-linear terms (in the anomalies) is a problematic step, as these are not obviously much smaller than some of the other terms. Nevertheless, we follow the linearization procedure to achieve a better comparability to the results of *Randel et al.* [2007] and *Schoeberl et al.* [2008] and to achieve further insight into the nature of in-mixing, keeping in mind the potential limitation of this analysis due to the above approximations. The equations for the annual mean $\langle\chi\rangle$ and the annual amplitude χ_a, resulting from linearizing equation (2), read

$$\partial_\theta \langle\chi\rangle = -\frac{\langle\widetilde{\alpha}\rangle}{\langle\dot{\theta}\rangle} \langle\chi\rangle + \frac{1}{\langle\dot{\theta}\rangle} \left[\langle P\rangle + \langle\alpha^i\rangle\chi_i\right], \tag{A3}$$

$$\partial_\theta \chi_a = -\frac{1}{\langle\dot{\theta}\rangle} (i\omega_a + \langle\widetilde{\alpha}\rangle)\chi_a - \frac{1}{\langle\dot{\theta}\rangle} \left[\alpha_a^n (\langle\chi\rangle - \chi_n) + \alpha_a^s (\langle\chi\rangle - \chi_s) + \dot{\theta}_a \partial_\theta \langle\chi\rangle\right], \tag{A4}$$

with $\langle\widetilde{\alpha}\rangle = \langle L\rangle + \langle\alpha^n\rangle + \langle\alpha^s\rangle$ and a vanishing annual amplitude assumed for photochemical production and loss (a valid approximation for O_3 and CO). The terms in the square brackets on the right-hand side of the amplitude equation (A4) represent the effects of the annual variation of in-mixing (α_a^i) and of the annual variation of upwelling ($\dot{\theta}_a$) acting on the meridional and vertical background gradients. *Randel et al.* [2007] assumed a negligible impact of in-mixing and balanced the $\dot{\theta}_a \partial_\theta \langle\chi\rangle$ term with the $i\omega_a\chi_a$ term. Equation (A4) is more general than this balance. Because equations (A3) and (A4) have the same form as equation (3), the solution for the mixing ratio annual mean and annual amplitude can be computed analogously as

$$\langle\chi\rangle(\theta) = \mathrm{e}^{-\int_{\theta_0}^{\theta} \gamma' \, \mathrm{d}\theta'} \int_{\theta_0}^{\theta} \left(\frac{\langle P\rangle + \langle\alpha^i\rangle\chi_i}{\langle\dot{\theta}\rangle} \right) \mathrm{e}^{\int_{\theta_0}^{\theta'} \gamma' \, \mathrm{d}\theta''} \mathrm{d}\theta' + \langle\chi_0\rangle \mathrm{e}^{-\int_{\theta_0}^{\theta} \gamma' \, \mathrm{d}\theta'}, \tag{A5}$$

$$\chi_a(\theta) = -\mathrm{e}^{-\int_{\theta_0}^{\theta} \tilde{\gamma}\, \mathrm{d}\theta'} \int_{\theta_0}^{\theta} \left(\frac{\alpha_a^n(\langle\chi\rangle - \chi_n) + \alpha_a^s(\langle\chi\rangle - \chi_s) + \dot{\theta}_a \partial_\theta \langle\chi\rangle}{\langle\dot{\theta}\rangle} \right) \cdot \mathrm{e}^{\int_{\theta_0}^{\theta'} \tilde{\gamma}\, \mathrm{d}\theta''} \mathrm{d}\theta' + \chi_{a\,0} \mathrm{e}^{-\int_{\theta_0}^{\theta} \tilde{\gamma}\, \mathrm{d}\theta'}, \quad \text{(A6)}$$

with $\gamma' = \frac{\langle\tilde{\alpha}\rangle}{\langle\dot{\theta}\rangle}$, $\tilde{\gamma} = \frac{i\omega_a + \langle\tilde{\alpha}\rangle}{\langle\dot{\theta}\rangle}$ and $\chi_{a\,0} = \chi_a(\theta_0)$.

[72] Equation (A5) shows that the annual mean profile is determined by the annual mean photochemical production and in-mixing rates. Equation (A6), on the other hand, shows that the annual amplitude at a particular θ-level is forced by the seasonality of upwelling $\dot{\theta}_a$ acting on the mean vertical gradient [cf. *Randel et al.*, 2007] and by the seasonality of in-mixing α_a^i acting on the mean horizontal gradient. Obviously, the sensitivity of the annual amplitude to upwelling is controlled by the mean vertical gradient $\partial_\theta\langle\chi\rangle$, the sensitivity to in-mixing by the mean horizontal (meridional) gradient $\langle\chi\rangle - \chi_i$. Hence, the annual amplitude is sensitive to in-mixing only for species with large meridional gradients. It should be noted, however, that the Eulerian equation (A6) not exactly isolates the effect of in-mixing on the annual amplitude, as it involves the annual mean background profile in both terms (vertical transport and in-mixing) which is, in turn, affected by both photochemical production and in-mixing via equation (A5).

[73] The second term on the right-hand side of equation (A6) shows the upward propagation of the annual amplitude signal $\chi_{a\,0}$ from θ_0 to θ. Note, that for ozone the annual amplitude in the lower TTL is very small (compare Figure 9a). For species with small vertical and horizontal gradients ($\partial_\theta\langle\chi\rangle \approx 0$ and $(\langle\chi\rangle - \chi_i) \approx 0$), like water vapor above the tropopause, this second term in equation (A6) is dominating and the tropical mixing ratio reads (in the case of only annual variations and, for simplicity, of constant upwelling and in-mixing rates)

$$\chi(t,\theta) = \chi_{a0} \mathrm{e}^{i\left(\omega_a t - \frac{\omega_a}{\langle\dot{\theta}\rangle}(\theta-\theta_0)\right)} \mathrm{e}^{-\frac{\langle\tilde{\alpha}\rangle}{\langle\dot{\theta}\rangle}(\theta-\theta_0)}. \quad \text{(A7)}$$

This is just the famous 'tape recorder' case with the first exponential representing the upward propagation of the lower boundary source function χ_{a0} and the second exponential the dilution of the phases due to in-mixing and chemical loss. *Schoeberl et al.* [2008] derived an equation analogous to equation (A7) for water vapor from the simplified balance of the left-hand side of equation (A4) with the first term on the right-hand side, $\partial_\theta\chi_a = -\frac{1}{\langle\dot{\theta}\rangle} i\omega_a\chi_a$. Our discussion generalizes the findings of *Schoeberl et al.* [2008] to non-vanishing in-mixing, as the following paragraph will show.

[74] In-mixing of extratropical air into the tropics may also cause a tape recorder behavior. For illustration, consider in-mixing confined to a small θ-layer around θ^*, with upwelling and in-mixing rates independent of θ. Inserting an in-mixing rate of the form $\alpha_a^i \cdot \delta(\theta - \theta^*)$ into equation (A6) yields (again, for simplicity, for constant upwelling and in-mixing rates)

$$\chi(t,\theta) = \tilde{\chi}_{0a} \mathrm{e}^{i\left(\omega_a t - \frac{\omega_a}{\langle\dot{\theta}\rangle}(\theta-\theta^*)\right)} \mathrm{e}^{-\frac{\langle\tilde{\alpha}\rangle}{\langle\dot{\theta}\rangle}(\theta-\theta^*)}, \quad \text{(A8)}$$

with $\tilde{\chi}_{0\,a} = (\chi_i - \langle\chi\rangle)\frac{\alpha_a^i}{\langle\dot{\theta}\rangle}\big|_{\theta=\theta^*}$, hence similar phase propagation and dilution factors as in equation (A7). Consequently, for suitable species the annual signal in-mixed at θ^* potentially propagates upwards. For ozone this is the case, as we discussed in section 4.2.

[75] **Acknowledgments.** We thank M. Volk and Bill Randel for helpful discussions and the ECMWF for providing the reanalysis data. F. Ploeger thanks COST for funding a Short Term Scientific Mission at DAMTP/Cambridge.

References

Avallone, L. M., and M. J. Prather (1997), Tracer-tracer correlations: Three-dimensional model simulations and comparisons to observations, *J. Geophys. Res.*, *102*, 19,233–19,246.

Chen, P. (1995), Isentropic cross-tropopause mass exchange in the extratropics, *J. Geophys. Res.*, *100*, 16,661–16,673.

Dee, D. P., et al. (2011), The ERA-interim reanalysis: configuration and performance of the data assimilation system, *Q. J. R. Meteorol. Soc.*, *137*, 553–597, doi:10.1002/qj.828.

Dunkerton, T. J. (1995), Evidence of meridional motion in the summer lower stratosphere adjacent to monsoon regions, *J. Geophys. Res.*, *100*(D8), 16,675–16,688.

Edwards, J. M., and A. Slingo (1996), Studies with a flexible new radiation code. I: Choosing a configuration for a large-scale model, *Q. J. R. Meteorol. Soc.*, *122*, 689–719, doi:10.1002/qj.49712253107.

Folkins, I., P. Bernath, C. Boone, G. Lesins, N. Livesey, A. M. Thompson, K. Walter, and J. C. Witte (2006), Seasonal cycles of O_3, CO, and convective outflow at the tropical tropopause, *Geophys. Res. Lett.*, *33*, L16802, doi:10.1029/2006GL026602.

Forster, P., and K. P. Shine (1999), Stratospheric water vapour change as possible contributor to observed stratospheric cooling, *Geophys. Res. Lett.*, *26*(21), 3309–3312, doi:10.1029/1999GL010487.

Fueglistaler, S., and P. H. Haynes (2005), Control of interannual and longer-term variability of stratospheric water vapor, *J. Geophys. Res.*, *110*, D24108, doi:10.1029/2005JD006019.

Fueglistaler, S., H. Wernli, and T. Peter (2004), Tropical troposphere-to-stratosphere transport inferred from trajectory calculations, *J. Geophys. Res.*, *109*, D03108, doi:10.1029/2003JD004069.

Fueglistaler, S., A. E. Dessler, T. J. Dunkerton, I. Folkins, Q. Fu, and P. W. Mote (2009a), Tropical tropopause layer, *Rev. Geophys.*, *47*, RG1004, doi:10.1029/2008RG000267.

Fueglistaler, S., B. Legras, A. Beljaars, J. J. Morcrette, A. Simmons, A. M. Tompkins, and S. Uppala (2009b), The diabatic heat budget of the upper troposphere and lower/mid stratosphere in ECMWF reanalysis, *Q. J. R. Meteorol. Soc.*, *135*, 21–37, doi:10.1002/qj.361.

Fueglistaler, S., P. H. Haynes, and P. M. Forster (2011), The annual cycle in lower stratospheric temperatures revisited, *Atmos. Chem. Phys.*, *11*, 3701–3711, doi:10.5194/acp-11-3701-2011.

Grooß, J.-U., and J. M. Russell (2005), Technical note: A stratospheric climatology for O_3, H_2O, CH_4, NO_x, HCl and HF derived from HALOE measurements, *Atmos. Chem. Phys.*, *5*, 2797–2807.

Haynes, P., and E. Shuckburgh (2000), Effective diffusivity as a diagnostic of atmospheric transport: 2. Troposphere and lower stratosphere, *J. Geophys. Res.*, *105*(D18), 22,795–22,810.

Haynes, P., C. J. Marks, M. E. McIntyre, T. G. Shepherd, and K. P. Shine (1991), On the downward control of extratropical diabatic circulations by eddy-induced mean zonal forces, *J. Atmos. Sci.*, *48*, 651–679.

Holton, J. R., and A. Gettelman (2001), Horizontal transport and the dehydration of the stratosphere, *Geophys. Res. Lett.*, *28*(14), 2799–2802.

Homan, C. D., C. M. Volk, A. C. Kuhn, A. Werner, J. Baehr, S. Viciani, A. Ulanovski, and F. Ravegnani (2010), Tracer measurements in the tropical tropopause layer during the AMMA/SCOUT-O3 aircraft campaign, *Atmos. Chem. Phys.*, *10*, 3615–3627.

Homeyer, C. R., K. P. Bowman, L. L. Pan, E. L. Atlas, R. S. Gao, and T. L. Campos (2011), Dynamical and chemical characteristics of tropospheric intrusions observed during START08, *J. Geophys. Res.*, *116*, D06111, doi:10.1029/2010JD015098.

Hoor, P., H. Wernli, M. I. Hegglin, and H. Boenisch (2010), Transport timescales and tracer properties in the extratropical UTLS, *Atmos. Chem. Phys.*, *10*, 7929–7944, doi:10.5194/acp-10-7929-2010.

James, R., M. Bonazzola, B. Legras, K. Surbled, and S. Fueglistaler (2008), Water vapor transport and dehydration above convective outflow during Asian monsoon, *Geophys. Res. Lett.*, *35*, L20810, doi:10.1029/2008GL035441.

Konopka, P., J.-U. Grooß, F. Ploeger, and R. Müller (2009), Annual cycle of horizontal in-mixing into the lower tropical stratosphere, *J. Geophys. Res.*, *114*, D19111, doi:10.1029/2009JD011955.

Konopka, P., J. U. Grooß, G. Günther, F. Ploeger, R. Pommrich, R. Müller, and N. Livesey (2010), Annual cycle of ozone at and above the tropical tropopause: Observations versus simulations with the Chemical Lagrangian Model of the Stratosphere (CLaMS), *Atmos. Chem. Phys.*, *10*, 121–132.

Legras, B., B. Joseph, and F. Lefèvre (2003), Vertical diffusivity in the lower stratosphere from Lagrangian back-trajectory reconstructions of ozone profiles, *J. Geophys. Res.*, *108*(D18), 4562, doi:10.1029/2002JD003045.

Legras, B., I. Pisso, G. Berthet, and F. Lefèvre (2005), Variability of the Lagrangian turbulent diffusion in the lower stratosphere, *Atmos. Chem. Phys.*, *5*, 1605–1622.

Marcy, T. P., et al. (2007), Measurements of trace gases in the tropical tropopause layer, *Atmos. Environ.*, *41*(34), 7253–7261, doi:10.1016/j.atmosenv.2007.05.032.

McKenna, D. S., P. Konopka, J.-U. Grooß, G. Günther, R. Müller, R. Spang, D. Offermann, and Y. Orsolini (2002), A new Chemical Lagrangian Model of the Stratosphere (CLaMS): 1. Formulation of advection and mixing, *J. Geophys. Res.*, *107*(D16), 4309, doi:10.1029/2000JD000114.

Mote, P. W., K. H. Rosenlof, J. R. Holton, R. S. Harwood, and J. W. Waters (1995), Seasonal variations of water vapor in the tropical lower stratosphere, *Geophys. Res. Lett.*, *22*, 1093–1096, doi:10.1029/95GL01234.

Mote, P. W., et al. (1996), An atmospheric tape recorder: The imprint of tropical tropopause temperatures on stratospheric water vapor, *J. Geophys. Res.*, *101*(D2), 3989–4006, doi:10.1029/95JD03422.

Mote, P. W., T. J. Dunkerton, M. E. McIntyre, E. A. Ray, P. H. Haynes, and J. M. Russell III (1998), Vertical velocity, vertical diffusion, and dilution by midlatitude air in the tropical lower stratosphere, *J. Geophys. Res.*, *103*, 8651–8666, doi:10.1029/98JD00203.

Ploeger, F., P. Konopka, G. Günther, J.-U. Grooß, and R. Müller (2010), Impact of the vertical velocity scheme on modeling transport in the tropical tropopause layer, *J. Geophys. Res.*, *115*, D03301, doi:10.1029/2009JD012023.

Ploeger, F., et al. (2011), Insight from ozone and water vapour on transport in the tropical tropopause layer (TTL), *Atmos. Chem. Phys.*, *11*, 407–419.

Pommrich, R., et al. (2010), What causes the irregular cycle of the atmospheric tape recorder signal in HCN?, *Geophys. Res. Lett.*, *37*, L16805, doi:10.1029/2010GL044056.

Pommrich, R., R. Müller, J. U. Grooß, P. Konopka, G. Günther, H.-C. Pumphrey, S. Viciani, F. D'Amato, and M. Riese (2011), Carbon monoxide as a tracer for tropical troposphere-to-stratosphere transport in the Chemical Lagrangian Model of the Stratosphere (CLaMS), *Geosci. Model Dev. Discuss.*, *4*, 1185–1211.

Pumphrey, H. C., C. Boone, K. A. Walker, P. Bernath, and N. J. Livesey (2008), Tropical tape recorder observed in HCN, *Geophys. Res. Lett.*, *35*, L05801, doi:10.1029/2007GL032137.

Randel, W. J., and M. Park (2006), Deep convective influence on the Asian summer monsoon anticyclone and associated tracer variability observed with Atmospheric Infrared Sounder (AIRS), *J. Geophys. Res.*, *111*, D12314, doi:10.1029/2005JD006490.

Randel, W. J., M. Park, F. Wu, and N. Livesey (2007), A large annual cycle in ozone above the tropical tropopause linked to the Brewer-Dobson circulation, *J. Atmos. Sci.*, *64*, 4479–4488.

Randel, W. J., M. Park, L. Emmons, D. Kinnison, P. Bernath, K. A. Walker, C. Boone, and H. Pumphrey (2010), Asian monsoon transport of pollution to the stratosphere, *Science*, *328*(5978), 611–613, doi:10.1126/science.1182274.

Ray, E. A., et al. (2010), Evidence for changes in stratospheric transport and mixing over the past three decades based on multiple data sets and tropical leaky pipe analysis, *J. Geophys. Res.*, *115*, D21304, doi:10.1029/2010JD014206.

Russell, J. M., L. L. Gordley, J. H. Park, S. R. Drayson, A. F. Tuck, J. E. Harries, R. J. Cicerone, P. J. Crutzen, and J. E. Frederick (1993), The Halogen Occultation Experiment, *J. Geophys. Res.*, *98*, 10,777–10,797, doi:10.1029/93JD00799.

Schiller, C., J.-U. Grooß, P. Konopka, F. Ploeger, F. H. S. dos Santos, and N. Spelten (2009), Hydration and dehydration at the tropical tropopause, *Atmos. Chem. Phys.*, *9*, 9647–9660.

Schmidt, T., J. Wickert, G. Beyerle, and C. Reigber (2004), Tropical tropopause parameters derived from GPS radio occultation measurements with CHAMP, *J. Geophys. Res.*, *109*, D13105, doi:10.1029/2004JD004566.

Schmidt, T., J. Wickert, and A. Haser (2010), Variability of the upper troposphere and lower stratosphere observed with GPS radio occultation bending angles and temperatures, *J. Adv. Space Res.*, *46*(2), 150–161, doi:10.1016/j.asr.2010.01.021.

Schoeberl, M. R., A. R. Douglass, Z. X. Zhu, and S. Pawson (2003), A comparison of the lower stratospheric age spectra derived from a general circulation model and two data assimilation systems, *J. Geophys. Res.*, *108*(D3), 4113, doi:10.1029/2002JD002652.

Schoeberl, M. R., B. Duncan, A. R. Douglass, J. Waters, N. J. Livesey, W. Read, and M. Filipiak (2006), The carbon monoxide tape recorder, *Geophys. Res. Lett.*, *33*, L12811, doi:10.1029/2006GL026178.

Schoeberl, M. R., et al. (2008), QBO and annual cycle variations in tropical lower stratosphere trace gases from HALOE and Aura MLS observations, *J. Geophys. Res.*, *113*, D05301, doi:10.1029/2007JD008678.

Simmons, A., S. Uppala, S. Dee, and S. Kobayashi (2006), ERA-Interim: New ECMWF reanalysis products from 1989 onwards, *ECMWF Newsl.*, *110*, 25–35.

Solomon, S., K. H. Rosenlof, R. W. Portmann, J. Daniel, S. M. Davis, T. J. Sanford, and G. K. Plattner (2010), Contributions of stratospheric water vapor to decadal changes in the rate of global warming, *Science*, *327*, 1219–1223.

Thompson, A. M., et al. (2003), Southern hemisphere additional ozonesondes (SHADOZ) 1998–2000 tropical ozone climatology: 2. Tropospheric variability and the zonal wave-one, *J. Geophys. Res.*, *108*(D2), 8241, doi:10.1029/2002JD002241.

Thompson, A., J. C. Witte, C. Jacquelyn, H. G. J. Smit, S. J. Oltmans, B. J. Johnson, V. W. J. H. Kirchhoff, and F. J. Schmidlin (2007), Southern hemisphere additional ozonesondes (SHADOZ) 1998–2004 tropical ozone climatology: 3. Instrumentation, station-to-station variability, and evaluation with simulated flight profiles, *J. Geophys. Res.*, *112*, D03304, doi:10.1029/2005JD007042.

Tuck, A. F., et al. (1997), The Brewer-Dobson circulation in the light of high altitude in situ aircraft observation, *Q. J. R. Meteorol. Soc.*, *123*, 1–69.

Uppala, S., S. Dee, S. Kobayashi, P. Berrisford, and A. Simmons (2008), Toward a climate data assimilation system: status update of ERA-Interim, *ECMWF Newsl.*, *115*, 12–18.

Volk, C. M., et al. (1996), Quantifying transport between the tropical and midlatitude lower stratosphere, *Science*, *272*, 1763–1768.

Walters, D. N., et al. (2011), The Met Office Unified Model Global Atmosphere 3.0/3.1 and JULES Global Land 3.0/3.1 configurations, *Geosci. Model Dev.*, *4*, 919–941, doi:10.5194/gmd-4-919-2011.

Yulaeva, E., J. R. Holton, and J. M. Wallace (1994), On the cause of the annual cycle in tropical lower-stratospheric temperatures, *J. Atmos. Sci.*, *51*, 169–174.